RBM47 is a Critical Regulator of Mouse Embryonic Stem Cell Differentiation

Pavan Kumar Mysuru Shivalingappa
National Centre For Cell Science
Divya Kumari Singh
National Centre For Cell Science
Vaishali Sharma
National Centre For Cell Science
Vivek Arora
National Centre For Cell Science
Anjali Shiras
National Centre For Cell Science
Sharmila Bapat (sabapat@nccs.res.in)
National Centre For Cell Science https://orcid.org/0000-0002-9557-2233

Research Article

Keywords: RNA binding motif 47 (RBM47), embryonic stem (ES) cells, ES cell differentiation, early embryonic development, primitive endoderm fate, FGF4-ERK pathway

Posted Date: March 21st, 2022

DOI: https://doi.org/10.21203/rs.3.rs-1452998/v1

Abstract

RNA-binding proteins (RBPs) are pivotal for regulating gene expression as they are involved in each step of RNA metabolism. Several RBPs are essential for viable growth and development in mammals. RNA-binding motif 47 (RBM47) is an RRM-containing RBP whose role in mammalian embryonic development is poorly understood, yet deemed to be essential since its loss in mouse embryos leads to perinatal lethality. In this study, we attempted to elucidate the significance of RBM47 cell-fate decisions of mouse embryonic stem cells (mESCs). Downregulation of *Rbm47* did not affect mESC maintenance and the cell cycle but perturbed the expression of primitive endoderm (PrE) markers. The PrE misregulation, however, could be reversed by either FGFR or MEK inhibitor suggesting an implication of RBM47 in regulating FGF-ERK signaling. Further, lineage-specific differentiation experiments revealed that *Rbm47* is essential for neuroectodermal and endodermal differentiation. Taken together, our study thereby assigns a hitherto unknown role(s) to RBM47 in a subtle regulation of mESC differentiation.

Introduction

Mammalian embryogenesis is initiated with the formation of a totipotent single-cell zygote, which embarks on a complex sequence of events that involve the establishment of diverse cellular types, intercellular interactions, mechanical and chemical cues that guide the patterning of tissues and organs to generate an entire individual [1, 2]. Mechanistic errors and perturbations during these events lead to embryo defects that sometimes prove to be lethal. Pre-implantation stage mammalian embryos have been successfully cultured *in vitro* and used to study cell dynamics of the early days of mammalian development. However, the precise course of events in post-implantation stages where the basic body plan is laid down remains the black box of embryonic development due to inaccessibility and associated experimental intricacies within the uterus [2].

Recent advances in the *in vitro* stem cell-derived embryo models have posed an exceptional avenue for recapitulating *in vivo* events of mammalian embryogenesis, lineage specification, tissue, and organ formation [1, 3]. The most widely used models are embryonic stem cells (ESCs) and induced pluripotent stem cells (iPSCs), which divide clonally and differentiate into all cell types. Recent studies have demonstrated the potential of ESCs to self-assemble and self-organize into embryo-like structures that mimic in vivo embryonic morphogenesis [1, 4–6]. In addition to modeling early embryonic development, the genetically modified ESCs are used to develop efficient protocols for differentiation into clinically relevant cell types, elucidate the significance of novel factors, and understand the fundamental processes governing pluripotency. Several studies have thus successfully explained transcriptional factors and their networks governing pluripotency [7]. However, there is increasing evidence for the RNA-based regulation of pluripotency and differentiation through the coordinated interplay between RBPs, cellular mRNAs, and non-coding RNAs [8, 9]. As RNA binding proteins (RBPs) are involved in every process of RNA regulation, several recent studies have emphasized their essential functions in the regulation of pluripotency and differentiation [10–16].

RNA-binding motif 47 (RBM47) is a novel, vertebrate-conserved RBP that contains three RNA-recognition motifs (RRM) that perform multifaceted roles in RNA editing, early embryonic development, and cancer [17]. In zebrafish, the depletion of *rbm47* in the embryos led to the upregulation of *wnt8a* that affected the head formation [18] and homozygous inactivation of *Rbm47* in mouse embryos caused perinatal lethality where embryos were lost particularly after the E10 stage due to fetal resorption [19]. To understand the function of *Rbm47* in ESCs, we interrogated publicly available datasets. We found that RBM47 was preferentially enriched in mRNA interactome of mESCs (Supplementary Fig. 1A; Kwon *et al.*, 2013). During the fibroblast reprogramming, there was surge in *Rbm47* expression, particularly in the late phase of reprogramming (day 12 - day 15) and remained high in the stable iPSCs compared to fibroblasts (Supplementary Fig. 1B and 1C; Hansson *et al.*, 2012; Polo *et al.*, 2012). A recent study identified two late-phase specific alternative splicing events regulated by RBM47 but didn't reveal their importance in maintaining the pluripotent state [23]. It was reported previously that RBM47 binds to *Nanog* mRNA in mouse ESCs, however the outcome of this interaction was not explained [24]. In the present study, we address some of the current gaps in understanding the function of *Rbm47* in mammalian embryonic development using mESC-based models (Fig. 1A). Depletion of *Rbm47* in mESCs using specific short hairpin RNAs (shRNAs) did not affect the self-renewal and cell cycle regulation as revealed by a lack of change in pluripotency markers; however various primitive endoderm (PrE) makers were upregulated in these sh*Rbm47* mESCs. The PrE bias was rescued in sh*Rbm47* mESCs by treating with MEK inhibitor or FGFR inhibitor, suggesting a role for RBM47 in modulating the FGF-ERK pathway in mESCs. Moreover, the skew towards PrE persisted when these cells were differentiated into multiple lineages by serum treatment, with a compromised neuroectoderm. Consequently, sh*Rbm47* mESCs displayed a significantly regressed teratoma as compared to control ESCs (sh*lacZ*). Lineage-specific differentiation experiments revealed that *Rbm47* is necessary for proper differentiation into neuroectodermal and endodermal lineages. Together, our findings reveal a novel role for *Rbm47* in cell fate decisions during early embryonic development.

Materials And Methods

Cell culture

AB 2.2 mESC line was a kind gift from the Wellcome Sanger Institute, Hinxton, UK. Mouse ESCs were cultured under feeder-free conditions on 0.2% gelatin as attachment factor in serum-free ESC medium: knockout DMEM supplemented with 15% KOSR, 1x non-essential amino acids, 1x glutamax, 0.1 mM β-mercaptoethanol, 50U/mL penicillin-streptomycin and 10 ng/mL leukaemia inhibitory factor (LIF). Cells were plated at a density of 2.0-2.5 x 10^4 live cells per cm^2 for routine cultures; medium was replenished every day and dissociated on the third day using accutase for passaging. All the experiments were performed using cells grown between passage 18 and 30 and were regularly tested for mycoplasma contamination using the TaKaRa PCR mycoplasma detection set (cat. no. 6601). Before lineage-specific differentiation, wild-type ES cells were grown for at least 2 passages in ESC + 2i medium: ESC medium supplemented with 3 μM CHIR99021 (Sigma-Aldrich) and 1 μM PD0325901 (Sigma-Aldrich). For

FGF4/ERK pathway modulation, ESC medium was supplemented with either DMSO, 1 μM PD0325901, or 100 PD173074 (Sigma-Aldrich). The protocols followed for ESC differentiation are provided in supplementary methods.

Plasmids, lentivirus preparation, and transduction

Plasmids used for lentivirus preparation were as follows: pLKO.1-TRC cloning vector was a gift from David Root (RRID:Addgene_10878); psPAX2- packaging plasmid & pMD2.G- envelop encoding plasmid were gifts from Didier Trono (RRID: Addgene_12260 and Addgene_12259 respectively). pLKO.1-TRC plasmid was digested with *AgeI* and *EcoRI* and the 7 kb fragment was gel purified and quantified. Sequences of shRNA oligos were obtained from The RNAi Consortium (TRC) public portal from Broad Institute (https://portals.broadinstitute.org/gpp/public/). Forward and reverse oligos were reconstituted at a concentration of 0.1nmol/µL and the annealing mixture of 25 µL was prepared by adding 11.25 µL of both the oligos and 2.5 µL 10x annealing buffer (1M NaCl, 100mM Tris-HCl pH 7.4 or NEB Buffer 2). The annealing mixture was placed in boiling water and gradually cooled to room temperature. The annealing mixture was diluted 100 times using 0.5x annealing buffer. 1 µL of 1:100 diluted mixture along with 10–20 ng of linear pLKO.1-TRC was used for 20 µL ligation reaction using rapid ligation kit (Roche/NEB). Competent *E. coli* stbl3 strain was transformed using 10 µL ligation mixture. Sequences encoding shRNAs were confirmed by Sanger DNA sequencing using U6 promoter-specific primer. Sequence targeting *lacZ* (sh*lacZ*: 5'-TCGTATTACAACGTCGTGACT-3') was used as a non-targeting control. Three shRNAs were used to target *Rbm47* in mouse ESCs, however, sh*Rbm47*#1 (5'-CCCGCGTTCATACATTTCTAA-3') and sh*Rbm47*#3 (5'-CCGTCCAATAACTCCTGTGTA-3') showed better knockdown efficiency both at RNA and protein levels and hence considered further.

Lentiviruses were produced in HEK 293T cells grown in DMEM/F12 supplemented with 10% FBS. These cells were reverse transfected with lentiviral plasmids using lipofectamine 3000 (Invitrogen). DNA mix was prepared by diluting 2.5 µg pLKO.1-shRNA plasmid, 2 µg psPAX2 and 1 µg pMD2.G in Opti-MEM (Gibco) or any serum-free basal medium to a volume of 243 µL and followed by 7 µL P3000 reagent. The lipid mix was prepared in a separate tube by diluting 7 µL Lipofectamine 3000 reagent in 243 µL Opti-MEM. DNA-lipid mix was obtained by dropwise addition of the DNA mix to the lipid mix. The contents were gently mixed with a pipette and incubated inside the hood for 10 minutes. Meanwhile, HEK 293T cells were dissociated with trypsin, harvested, and re-suspended in the complete medium. DNA-lipid mix along with 5–6 x 10^6 293T cells were plated per transfection in a 60 mm dish pre-coated with 0.2% gelatin and incubated overnight. The next day, the spent medium was replaced with 3–4 mL fresh complete medium. Supernatants were collected at 24 h and 48 h time points and pooled. The pooled supernatant was next passed through a 0.45 µm filter to remove cell debris and concentrated using Lenti-X concentrator (TaKaRa cat. no. 631231) following the manufacturer's instructions. The viral pellet was suspended in a 300 µL ESC medium and used for transduction, or aliquots were stored in -80^{o}C.

Mouse ESCs were transduced on a 6-well dish at the time of plating with different doses of virus concentrate suspended in ESC medium containing 6 µg/ mL polybrene and incubated for 16–24 h.

Cultures were fed with fresh medium and grown for another day. Next, cells were selected with a medium containing 1 µg/ mL puromycin until the mock-transduced cells (no virus) completely died. MOI was determined by counting the virus-transduced and control cells (no virus/no puromycin) as previously described [25]. The polyclonal population that yielded MOI of ~ 1 was used for further studies.

Rna Isolation And Reverse Transcription-quantitative Real-time Pcr (Rt-qpcr)

Total RNA was isolated from all the cell types by adding the appropriate amount of TRIzol Reagent (Cat. No. 15596-018; Ambion, life technologies) following the manufacturer's protocol. Quantification of isolated total RNA was done using a DeNovix spectrophotometer. Total RNA (0.5 -1.0 µg) was reverse transcribed into cDNA using Verso cDNA synthesis kit (Thermo Scientific). RT-qPCR was set up in duplicates or triplicates per sample with a reaction volume of 10 µL containing 2.5 µL of 1:25 diluted cDNA as template, 0.4 µM each forward and reverse primer and PowerUp SYBR green master mix (Applied biosystems A25743) and run in Quantstudio 6 Flex (Thermo Scientific). A four-stage thermocycling protocol (fast cycling mode) was employed. Briefly, stage I (hold) – 2 min at 50^0C for activation of UDG, Stage II (hold)- 2 min at 95^0C for activation of dual-lock DNA polymerase, stage III (40 cycles)- 95^0 C melt for 3s and 60^0 C anneal/extend for 30 s and Stage IV (post-amplification melt curve analysis)- the ramp (auto mode) was initiated from 60^0 C to 95^0 C. Melting curve was monitored in each run to determine the specificity of amplification. Unless otherwise stated, all the data were normalized to multiple endogenous controls- *18S rRNA, Actb*, and *Gapdh* and relative quantification (RQ) of target gene expression were performed as described previously [26]. RQ plots were represented as mean ± S.D or S.E.M as described in the figure legends.

Immunocytochemistry

Mouse ESCs were plated in 96-well optical-bottom plates (Nunc 165305) coated with 0.2% gelatin. The spent medium was removed and cells were washed with PBS. Cells were fixed in 4% phosphate-buffered formaldehyde for 15 minutes at room temperature and washed thrice with PBS. Cells were permeabilized and blocked for 30 minutes in PBS containing 5% BSA + 0.2% Triton-X. Cells were incubated with primary antibodies (supplementary table 3) diluted with antibody dilution buffer (PBS containing 1% BSA + 0.05% Triton-X) for one hour at room temperature. Excess antibodies were removed by rinsing with PBS thrice, cells were incubated with fluorophore-conjugated appropriate secondary antibodies diluted in antibody dilution buffer, washed thrice with PBS and nuclear staining was done with mounting medium containing DAPI and anti-fade agent DABCO (Sigma). Samples were imaged in Thermo Scientific CellInsight CX7 LZR High Content Analysis (HCA) platform using wide-field or confocal applications. Images were processed further using ImageJ software.

Teratoma Formation

In vivo differentiation potential of ESCs stably expressing either sh*lacZ* or sh*Rbm47* was tested by subcutaneously injecting $1x10^6$ cells suspended in 100 µL knockout-DMEM into the dorsal flank of 8-week old NOD/SCID mice.

Mice were regularly monitored for teratoma formation and euthanized between 4–5 weeks for harvesting teratomas. Teratoma dimensions were recorded using a Vernier caliper and the ellipsoid volume, V= ½ (Length*Width^2) was calculated [27]. Teratomas were fixed in 4% formaldehyde in PBS at 4^0 C overnight, embedded in paraffin and the sections were stained with hematoxylin and eosin for histological analysis.

Statistics

For cell culture-related experiments, the biological replicates indicate the samples collected from different culture dishes/wells at different times. GraphPad Prism 8.2.1 (441) was used to plot graphs and to perform statistical analysis. The student's t-test was used to compare differences between two groups and one-way ANOVA followed by posthoc tests for comparing three or more groups. Relevant information about statistical tests used, the number of replicates, and precision measures are mentioned in each figure legend. Statistical significance was described as follows: non-significant (ns) $p > .0.05$, * $p < 0.05$, ** $p < 0.01$, *** $p < 0.001$, **** $p < 0.0001$.

Results

Rbm47 **is abundantly expressed in pluripotent stem cells (PSCs) and localizes to both nucleus and cytoplasm**

We found that *Rbm47* transcript and protein were abundantly expressed in mESCs as compared with differentiated cells such as mouse embryonic fibroblasts (MEF) (Fig. 1B and 1C). To determine the cellular localization of RBM47 protein, we fractionated mouse ESCs into cytoplasmic and nuclear extracts and analyzed them by immunoblotting (Fig. 1D). RBM47 was found to be expressed as both, a nuclear and a cytoplasmic RBP with significant enrichment in the nucleus of mESCs, indicating its discrete roles in nuclear and cytoplasmic RNA metabolism. Similar data were obtained with human iPSC lines and human dermal fibroblasts suggesting closely related functions in human counterparts (Supplementary fig. S1 D, E, and F).

Rbm47 **expression profile in specific lineages derived** in vitro **from mESCs**

Early mouse development involves the specification of three lineages at the blastocyst stage. As shown in Fig. 1A, the early blastocyst stage (E3.25) has a fully specified outer layer of cells called trophectoderm (TE), while the inner cell mass (ICM) retains pluripotency. In the late blastocyst stage (E4.5), ICM undergoes lineage specification into the pluripotent epiblast (Epi) and primitive endoderm (PrE). As the

blastocyst enters the subsequent stages of development, TE gives rise to the extraembryonic ectoderm (ExE), and the PrE gives rise to visceral endoderm surrounding both the Epi and ExE. Epi gives rise to tri-lineages of the embryo proper. Fortunately, the self-renewing ability of these cells enabled us to derive and maintain stem cell lines from each of these lineages and utilize them to study blastocyst development in vitro [3]. ESCs can be derived from both the ICM and Epi and cultured indefinitely *in vitro* under defined growth conditions. Currently, protocols are available to convert mESCs into naive endoderm (nEnd) or extraembryonic endoderm (EXEn; similar to PrE) and epiblast-like cells (EpiLCs, similar to Epi) in addition to the traditional germ layer differentiation of embryo proper.

To explore the function of *Rbm47* during early embryonic development using mESCs, we subjected mESCs to various differentiation strategies and analyzed *Rbm47* expression. First, we differentiated mESCs as embryoid bodies (EBs), which undergo spontaneous differentiation into the three germ layers and mimic post-implantation embryos in vitro. RT-qPCR profiling revealed a 2–3 fold upregulation of *Rbm47* expression in differentiating EBs compared with ESCs (Fig. 1E). However, RBM47 protein level was correlated with mRNA only in 3 days-old EBs and gradually decreased during further EB differentiation (Fig. 1F). Expression of *Nanog*, a core pluripotency marker, significantly reduced both at mRNA and protein levels, served as an indicator for EB differentiation (Fig. 1E and 1F).

Next, to investigate whether *Rbm47* undergoes lineage-specific regulation, we converted mESCs into extraembryonic endoderm (cXEN) cells, epiblast-like cells (EpiLCs), definitive endoderm (DE), mesoderm (MES), and neuroectoderm (NE) and profiled its expression both at RNA and protein level (Fig. 1G and 1H). All the cultures were additionally profiled for expression of specific-lineage markers to ensure proper differentiation (Fig. 1H and Supplementary fig. S2). We observed that *Rbm47* mRNA was differentially expressed in cXEN and EpiLC, which mimic successive cell-fates of ICM post-implantation. In cXEN cells, *Rbm47* mRNA was upregulated nearly two-fold, whereas, in EpiLCs, it was downregulated (Fig. 1G). Interestingly, RBM47 protein level correlated significantly with mRNA level in EpiLC but not in cXEN as protein level was reduced compared to ESCs (Fig. 1H), indicating a possibility of post-transcriptional regulation of *Rbm47* in cXEN cells.

To gain insights into *Rbm47* expression in the lineages of the embryo proper, we analyzed mRNA and protein levels in mESC-derived DE, MES, and NE. We found that both *Rbm47* mRNA and protein levels were upregulated in the DE (Fig. 1G and 1H). In contrast, the expression was compromised significantly in MES and NE compared to ESCs (Fig. 1G and 1H). Together, these results suggest that *Rbm47* expression is subjected to lineage-specific gene regulation, with an increase at the protein level in DE and a concurrent decrease in other lineages compared to mESCs.

Rbm47 depletion doesn't affect in vitro mESC maintenance

We used the RNAi approach for loss-of-function studies to investigate the significance of *Rbm47* expression in mESCs. We transduced ESCs with lentivirus that expresses shRNAs targeting either *Rbm47* mRNA or *lacZ* mRNA (non-targeting control) and established stable cell lines (*Rbm47* depleted mESCs designated as sh*Rbm47*#1 and sh*Rbm47*#3; control ESCs as sh*lacZ* in the figures). There was an

efficient knockdown of *Rbm47* at mRNA (~ 80%) as well as protein levels (~ 50%) (Figs. 2A and 2B). *Rbm47*-depleted mESCs displayed no apparent change in the undifferentiated state as they expressed similar levels of pluripotency markers as control mESCs as demonstrated by RT-qPCR, western blotting, and immunocytochemistry (Figs. 2E, 2F, and 2G). The cell cycle profile of these mESCs was similar to that of control mESCs (Fig. 2H). In terms of morphology and alkaline phosphatase (ALP) activity, sh*Rbm47*#3 mESCs were comparable to control mESCs, whereas sh*Rbm47*#1 mESCs showed a slightly diffused morphology with a reduced intensity of ALP staining (Fig. 2C and 2D). However, these cells display a similar pluripotency marker profile as control mESCs. Overall, our data suggest that *Rbm47* is not necessary to maintain the pluripotent state of mESCs.

Downregulation of Rbm47 increases primitive endoderm (PrE)-like cells in mESC culture and FGF-ERK pathway inhibition rescues the effect

Since *Rbm47* depletion didn't affect the pluripotency and self-renewal of mESCs, we next considered analyzing the expression of differentiation markers specific to PrE, mesendoderm, TE, and neuroectoderm. Previously, it was established that mESC cultures display heterogeneity and comprise a subpopulation of lineage-committed cells [28, 29]. RT-qPCR revealed a significant upregulation of PrE markers *Gata6, Gata4, Sox17, Dab2, Pdgfra*, and *Foxa2* in sh*Rbm47* mESCs as compared with control mESCs (Fig. 3A and 3B). Expression of mesendodermal markers largely remained unchanged while a few neuroectodermal markers (*Pax6, Nestin*, and *Emx1*) were marginally downregulated. Most importantly, immunostaining revealed that *Rbm47*-depleted mESCs contained a higher fraction of GATA4 + PrE-like cells (sh*Rbm47*#1: 5.5% ± 2.3%; sh*Rbm47*#3: 6% ± 0.67%) as compared with control mESCs (sh*lacZ*: 2.2% ± 0.9%) (Fig. 3C and 3D).

Since ESCs are *in vitro* models of the ICM, the cells are routinely cultured in a medium supplemented with leukemia inhibitory factor (LIF). However, they can be converted to a hypomethylated ground state of pluripotency (similar to preimplantation ICM) by culturing in a medium containing inhibitors of GSK3ß and MEK1/2 (termed as '2i') [30]. To determine whether a return to the ground state would reverse *Rbm47*-depletion induced priming towards the PrE lineage, we cultured control and *Rbm47*-depleted mESCs for two passages in ‘2i’ supplemented ESC medium and analyzed these for PrE marker expression. We indeed observed that culture conditions capturing the ground state were sufficient to reverse the PrE priming in *Rbm47*-depleted ESCs (Supplementary Fig. 3).

It is well-documented that FGF4-ERK signaling is the central pathway in cell-fate determination of the ICM into NANOG-positive Epi and GATA6-positive PrE at the E4.5 stage of the mouse blastocyst (Fig. 3E). Blocking FGF signaling with inhibitors of FGF receptor (FGFR) and ERK is reported to convert ICM into Epi [31]; in contrast, overactivation of FGF signaling can transform ICM to PrE [32]. To assess the possible effect of *Rbm47* depletion in modulating the FGF-ERK pathway, we treated sh*Rbm47* mESCs with

PD0325901 (MEK1/2 inhibitor, MEKi) or PD173074 (Pan-FGFR inhibitor, FGFRi) for 48 h and profiled for expression of PrE markers by RT-qPCR and GATA4 immunostaining. The use of either inhibitor reduced the PrE marker levels significantly, suggesting the FGF-ERK signaling is implicated in increasing PrE-like subpopulation in *Rbm47*-depleted mESCs (Fig. 3F and 3I). Further, to confirm the activation of this pathway, we quantified the expression of *Fgfr1, Fgfr2*, and *Fgf4* mRNAs in *Rbm47*-depleted mESCs; however, there was no significant change in the mRNA levels of the FGF receptors and the ligand as compared with control cells (Fig. 3G). Additionally, we did not observe a spike in phospho-ERK1/2 levels in *Rbm47*-depleted ESCs, a direct measure of FGF signaling (Fig. 3H). Collectively, our findings demonstrate that *Rbm47*-depleted ESCs displayed upregulated PrE related genes and contained an increased population of GATA4 + cells compared to control ESCs. Culturing these cells in ESC medium supplemented with either 2i, MEKi, or FGFRi could reverse the priming towards PrE, indicating the implication of *Rbm47* in regulating the FGF-ERK pathway.

Rbm47 depleted ESCs do not retain a complete multi-lineage differentiation potential

To evaluate the role *Rbm47* on differentiation potential of mESCs *in vivo*, we xenografted sh*lacZ* and sh*Rbm47* mESCs subcutaneously into NSG mice for teratoma formation. *Rbm47*-depleted ESCs formed significantly smaller teratomas (mean teratoma volume: sh*Rbm47*#1 = 251.63 mm^3; sh*Rbm47*#3 = 324.6 mm^3) compared to control ESC-derived teratoma (mean teratoma volume: 2081.36 mm^3), indicating that *Rbm47* might be necessary for self-renewal during the differentiation of mESCs (Fig. 4A and 4B). However, sectioning and histological observation of these teratomas revealed that *Rbm47*-depleted mESCs could form structures from all three germ layers despite the drastic gross reduction in teratoma size (Fig. 4C). Next, to assess the multi-lineage differentiation potential of sh*Rbm47* mESCs *in vitro*, we measured the expression of various markers in six-day serum differentiated monolayer cultures. As shown in Fig. 4D, there was no consistent variation in the transcripts of mesendoderm, but extraembryonic endoderm (ExEn; similar to PrE) markers (*Gata6, Gata4, Pdgfra, Foxa2, and Sox17*) were consistently upregulated, while neuroectoderm progenitor markers (*Nestin, Pax6, and Cdh2*) were downregulated in *shRbm47* mESCs as compared with control cells. These data indicate that *Rbm47* depleted ESCs exhibit a skewed multi-lineage differentiation potential and might have an enhanced tendency for differentiating into ExEn lineage with compromised neuroectodermal and mesendodermal fate.

Lineage-specific differentiation reveals Rbm47 is essential of neuroectoderm and endoderm fate of ESCs

To further probe the effects of *Rbm47* depletion on differentiation, we profiled the expression of lineage-specific markers in sh*Rbm47* and control mESCs differentiated into definitive endoderm (DE), mesoderm (MES), and neuroectoderm (NE). As shown in Fig. 1G and 1H, *Rbm47* expression undergoes lineage-specific modulation, and the mRNA and protein levels were notably upregulated in wild-type mESC-derived DE. To determine whether *Rbm47* is essential for DE formation, we plated control and sh*Rbm47* mESCs to form EBs for 2-days in the serum-free formulation and then directed to DE lineage by supplementing the medium with Activin A. We observed that *Rbm47*-depleted EBs were significantly

smaller and irregularly shaped than the control EBs (Fig. 5A and 5B). RT-qPCR profiling revealed a consistent downregulation of definitive endoderm markers (*Sox17, Foxa2*, *Cdh1*, and *Hhex)* (Fig. 5E), suggesting *Rbm47* is necessary for proper differentiation of mESCs to DE.

We next specified *Rbm47*-depleted ESCs to MES by treating 2-day old EBs with Activin A, VEGF, and BMP4 for two days. A role for *Rbm47* in the mesodermal specification was not expected since it was significantly downregulated in wild-type mESC-derived MES (Fig. 1G and 1H) and undetected in mesodermal tissues embryo and adult mouse [33]. However, surprisingly, *Rbm47*-depleted ESCs not only formed significantly smaller EBs (Fig. 5C and 5D) but also displayed enhanced expression of mesodermal markers such as *Mixl1, Kdr, Gsc, Mesp1*, and *Hand1* (Fig. 5F).

On the other hand, the involvement of *Rbm47* in neuroectodermal differentiation was indicated since critical NE progenitor markers (*Pax6, Nestin*, and *Cdh2*) were suppressed upon *Rbm47* depletion (Fig. 3A and 4D), we expected to be necessary for proper NE differentiation. As expected, we observed a significant decrease in self-renewal of *Rbm47*-depleted mESCs on day 2 of NE induction with N2B27-high insulin medium, and the effect persisted throughout the duration (day 8) (Fig. 5G). RT-qPCR analysis and immunocytochemistry of NE-differentiated sh*Rbm47* mESCS revealed a significant downregulation of most NE markers, with a clear bias towards ExEn markers as compared with control mESCs (Fig. 5I). Immunostaining of these cultures with NE markers PAX6 and TUBB3 (B-3-Tubulin) and ExEn marker GATA4 correlated with the RT-qPCR data (Fig. 5H). Collectively, our findings from the lineage-specific differentiation models successfully demonstrated that *Rbm47* is essential for fine-tuning the cell-fate decisions and lineage specification of mESCs. *Rbm47* depletion strongly affects the DE and NE differentiation programs.

Discussion

RBM47 is a multifunctional RNA-binding protein conserved in vertebrates, which has been suggested to be essential for development, C to U RNA editing, and tumor suppression [17]. Amongst these, previous investigations have clearly defined the role of RBM47 as a tumor suppressor and as a cofactor for APOBEC1-mediated C to U RNA editing in mammals [33, 34]. However, its role in mammalian development is poorly elucidated. In mouse embryos, Fossat et al. showed that one functional allele of *Rbm47* is necessary for viability and postnatal growth of the embryo proper [19]. Inactivation of both *Rbm47* alleles resulted in the loss of embryos due to fetal resorption after mid-gestation.

The present study used mouse ESCs and lineage-specific differentiation methods as *in vitro* tools to understand the principal causes for perinatal lethality in *Rbm47*-inactivated mouse embryos. Profiling of *Rbm47* expression in mESC-derived lineages indicated downregulation of both *Rbm47* mRNA and protein in EpiLCs, while in cXEN cells, mRNA level increased significantly, but protein level didn't correlate with mRNA, suggesting an exciting possibility of post-transcriptional regulation in ExEn derivatives. Differentiation of mESCs to lineages of embryo proper, we found that *Rbm47* was remarkably

upregulated in definitive endoderm and downregulated in mesoderm and neuroectoderm derivatives at both mRNA and protein levels. In earlier studies with E8.5 embryos, *Rbm47* mRNA was strongly detected in endoderm and ExEn appendages like foregut and yolk sac but weakly detected in other developing tissues [33], indicating that our study using mESCs indeed recapitulated *in vivo* expression patterns. Furthermore, this spatial expression was correlated within adult mouse tissues as this protein was highly detected in the small intestine, pancreas, and liver but undetected in the brain, heart, and skeletal muscles [33]. The Genotype-Tissue Expression (GTEx) data (*GTEx Portal*, accessed on 2021-08-13) suggests that this tissue-specific expression pattern is conserved for human *RBM47*.

By generating *Rbm47*-knockdown mESCs, our study demonstrated that insufficient levels of RBM47 did not affect ESC maintenance as the cells displayed a similar profile for pluripotency markers and cell cycle. However, profiling these cells for lineage-specific differentiation markers indicated a dysregulation of PrE lineage marker expression. It is well-known that mESC cultures are heterogeneous and express a small fraction of lineage-committed metastable cells [28, 29]. We observed that *Rbm47* depletion induced a significant increase in GATA4 + PrE-like cells. There is clear evidence that FGF4-ERK signaling is the central pathway that converts pluripotent Epi (NANOG+) to PrE (GATA6/GATA4+) in developing embryos [31, 32]. We thus tested whether this pathway is implicated in *Rbm47* depleted cells. Profiling for expression of critical components of FGF signaling including *Fgfr1*, *Fgfr2*, and *Fgf4* did not indicate any significant changes, nor were the downstream effectors, phosphorylated ERK1/2, as compared with control cells. Interestingly, these cells were responsive to 2i, FGFRi, or MEKi supplemented medium and displayed reduced PrE markers and GATA4 + cells in culture. Studying how these cells still respond to FGF-ERK pathway inhibitors will be intriguing.

Since *Rbm47*-knockdown didn't affect mESC maintenance *in vitro*, we sought whether its depletion would affect multi-lineage differentiation potential. Teratoma formation assay indicated that although *Rbm47*-knockdown severely reduced the gross size, there were no overt skews among lineages and the knockdown teratomas contained primitive tissues from all three lineages. It is possible that the abnormalities or skews were not conclusively defined as we didn't obtain knockdown teratoma of similar size and maturation as control. Nevertheless, *in vitro* multi-lineage differentiation experiments hinted that *Rbm47* depletion affects multi-lineage potential of mESCs. Knockdown cells showed a predisposition towards ExEn lineage with an increased number of GATA4 + ExEn-like cells but affected neuroectodermal fate by decreasing the generation of PAX6 + neural progenitor cells. Further, by applying a definitive endoderm conversion protocol, we proved the relevance of *Rbm47* in the endoderm. As it is expressed mainly in endodermal lineages *in vivo*, we found that a sufficient level of RBM47 is necessary for endoderm cell-fate choice. Conversely, mesoderm conversion revealed that *Rbm47*-knockdown could enhance the expression of mesodermal markers, suggesting its crucial role in fine-tuning cell fate decisions during mESC differentiation.

Our study effectively recapitulated the significance of RBM47 in early mammalian development using mouse ESCs. We demonstrated its critical role in ESC differentiation into neuroectoderm and endoderm lineages. Further, in vivo studies are required to thoroughly understand the underlying aberrations that

caused the fetal resorption and perinatal lethality induced by *Rbm47* inactivation. Although our study is limited to deciphering its role in cell-fate decisions of ESCs, the insights would open new avenues for future investigations. RBM47 is a classical RNA-binding protein known to exert its function by regulating cellular mRNAs post-transcriptionally in various biological contexts. It is a novel regulator of alternative splicing besides stabilizing mRNA by binding to 3'-UTRs. Earlier studies have reported that undifferentiated ESCs possess a surplus of free ribosomes and subunits but are relatively poor in polysome abundance [36]. However, ESCs display a rapid surge in translation rate correlated with increased polysome activity in response to differentiation cues. Consequently, ESCs contain a reserve of lineage-related mRNAs that are not translated but are poised for a rapid translational leap. We believe RBM47 might play an essential role in regulating the quality of this mRNA pool and fine-tunes ES cell-fate decisions to the differentiation milieu. We envisage future studies that determine the target mRNA network of RBM47 in ESCs for a better understanding of critical molecular events it regulates during early embryonic development.

Declarations

Author contributions

Conceptualization: SAB, AS & PKMS; Funding acquisition: AS; Supervision: SAB & AS; Methodology: SAB, AS & PKMS; Investigation and formal analysis: PKMS (ES cell culture & experiments, RNA isolation, RT-qPCR, western blotting, immunostaining, molecular cloning) DKS (RNA isolation, RT-qPCR, cell cycle & western botting), VS (RNA isolation & RT-qPCR) & VA (RT-qPCR & plasmid screening); Writing - original draft preparation: PKMS and SAB; Writing - review and editing: SAB, PKMS. All authors commented on previous versions of the manuscript and read and approved the final manuscript.

Funding

This work was supported by the Department of Biotechnology, Government of India (BT/PR15178/MED/31/313/2015) and intramural funds from National Centre for Cell Science (NCCS). Junior and senior research fellowships were granted to: PKMS by University Grants Commission; DKS by Department of Biotechnology; VS by Indian Council of Medical Research. VA was supported by project grant BT/PR 10708.

Availability of data and material

The manuscript and its supplementary information file contain all the relevant data generated during this study.

Acknowledgements

We dedicate this research paper to the memory of our colleague the late Dr. Anjali Shiras, who unfortunately succumbed to COVID-19. We sincerely thank Prof. Alan Bradley & Wellcome Sanger Institute for providing AB2.2 mouse ESCs. We acknowledge Dr. Akaram Bagal, for his comments on

teratoma sections. We thank all the central facilities of NCCS and their staff for the support during the investigation.

Conflict of interest

The authors have no financial or proprietary interests in any material discussed in this article.

Ethical approval

Experiments on pluripotent stem cells (ESCs/iPSCs) were in compliance with the National Guidelines for Stem Cell Research (2013 & 2017) and ethical approval was granted by NCCS Institutional Committee for Stem Cell Research (ID: NCCS/IC-SCR/2016-I/3). Animal experiments were carried out as per CPCSEA guidelines and ethical approval was granted by the Institute's Animal Ethics Committee (ID: EAF/2015/B-253 & EAF/2019/B-351). Recombinant DNA technology used in the study was in compliance with Guidelines for Biosafety from Department of Biotechnology and ethical approval was granted by the Institutional Biosafety Committee (ID: 2015033 & 2018111).

References

1. Rossant J, Tam PPL (2021) Opportunities and challenges with stem cell-based embryo models. Stem Cell Reports 16:1031–1038. https://doi.org/10.1016/j.stemcr.2021.02.002
2. Shahbazi MN, Zernicka-Goetz M (2018) Deconstructing and reconstructing the mouse and human early embryo. Nat Cell Biol 20:878–887. https://doi.org/10.1038/s41556-018-0144-x
3. Zylicz JJ (2020) Defined Stem Cell Culture Conditions to Model Mouse Blastocyst Development. Curr Protoc Stem Cell Biol 52:1–11. https://doi.org/10.1002/cpsc.105
4. Veenvliet J V., Bolondi A, Kretzmer H, et al (2020) Mouse embryonic stem cells self-organize into trunk-like structures with neural tube and somites. Science (80-) 370:. https://doi.org/10.1126/science.aba4937
5. Rivron NC, Frias-Aldeguer J, Vrij EJ, et al (2018) Blastocyst-like structures generated solely from stem cells. Nat 2018 5577703 557:106–111. https://doi.org/10.1038/s41586-018-0051-0
6. Sahu S, Sharan SK (2020) Translating Embryogenesis to Generate Organoids: Novel Approaches to Personalized Medicine. iScience 23:101485. https://doi.org/10.1016/j.isci.2020.101485
7. Orkin SH, Hochedlinger K (2011) Chromatin connections to pluripotency and cellular reprogramming. Cell 145:835–850. https://doi.org/10.1016/J.CELL.2011.05.019
8. Wright JE, Ciosk R (2013) RNA-based regulation of pluripotency. Trends Genet 29:99–107. https://doi.org/10.1016/J.TIG.2012.10.007
9. Corsini NS, Peer AM, Moeseneder P, et al (2018) Coordinated Control of mRNA and rRNA Processing Controls Embryonic Stem Cell Pluripotency and Differentiation. Cell Stem Cell 22:543-558.e12. https://doi.org/10.1016/J.STEM.2018.03.002/ATTACHMENT/30C9A0AE-E728-4A09-9CE0-C689C7C233E1/MMC4.XLSX

10. Fagoonee S, Bearzi C, Di Cunto F, et al (2013) The RNA Binding Protein ESRP1 Fine-Tunes the Expression of Pluripotency-Related Factors in Mouse Embryonic Stem Cells. PLoS One 8:e72300. https://doi.org/10.1371/JOURNAL.PONE.0072300
11. Han H, Irimia M, Ross PJ, et al (2013) MBNL proteins repress ES-cell-specific alternative splicing and reprogramming. Nature 498:241–245. https://doi.org/10.1038/NATURE12270
12. Elatmani H, Dormoy-Raclet V, Dubus P, et al (2011) The RNA-binding protein Unr prevents mouse embryonic stem cells differentiation toward the primitive endoderm lineage. Stem Cells 29:1504–1516. https://doi.org/10.1002/STEM.712
13. Dvir S, Argoetti A, Lesnik C, et al (2021) Uncovering the RNA-binding protein landscape in the pluripotency network of human embryonic stem cells. Cell Rep 35:109198. https://doi.org/10.1016/J.CELREP.2021.109198
14. Li D, Kishta MS, Wang J (2020) Regulation of pluripotency and reprogramming by RNA binding proteins. Curr Top Dev Biol 138:113. https://doi.org/10.1016/BS.CTDB.2020.01.003
15. Ye J, Jin H, Pankov A, et al (2017) NF45 and NF90/NF110 coordinately regulate ESC pluripotency and differentiation. RNA 23:1270–1284. https://doi.org/10.1261/RNA.061499.117/-/DC1
16. Chen G, Zhang D, Zhang L, et al (2018) RBM14 is indispensable for pluripotency maintenance and mesoderm development of mouse embryonic stem cells. Biochem Biophys Res Commun 501:259–265. https://doi.org/10.1016/J.BBRC.2018.04.231
17. Shivalingappa PKM, Sharma V, Shiras A, Bapat SA (2021) RNA binding motif 47 (RBM47): emerging roles in vertebrate development, RNA editing and cancer. Mol Cell Biochem 2021 1–13. https://doi.org/10.1007/S11010-021-04256-5
18. Guan R, El-Rass S, Spillane D, et al (2013) rbm47, a novel RNA binding protein, regulates zebrafish head development. Dev Dyn 242:1395–1404. https://doi.org/10.1002/dvdy.24039
19. Fossat N, Radziewic T, Jones V, et al (2016) Conditional restoration and inactivation of Rbm47 reveal its tissue-context requirement for viability and growth. Genesis 54:115–122. https://doi.org/10.1002/dvg.22920
20. Kwon SC, Yi H, Eichelbaum K, et al (2013) The RNA-binding protein repertoire of embryonic stem cells. Nat Struct Mol Biol 20:1122–1130. https://doi.org/10.1038/nsmb.2638
21. Hansson J, Rafiee MR, Reiland S, et al (2012) Highly Coordinated Proteome Dynamics during Reprogramming of Somatic Cells to Pluripotency. Cell Rep 2:1579–1592. https://doi.org/10.1016/J.CELREP.2012.10.014/ATTACHMENT/BD2B3958-D120-410A-A770-B7621D69ED8A/MMC6.XLSX
22. Polo JM, Anderssen E, Walsh RM, et al (2012) A molecular roadmap of reprogramming somatic cells into iPS cells. Cell 151:1617–1632. https://doi.org/10.1016/j.cell.2012.11.039
23. Cieply B, Park JW, Nakauka-Ddamba A, et al (2016) Multiphasic and Dynamic Changes in Alternative Splicing during Induction of Pluripotency Are Coordinated by Numerous RNA-Binding Proteins. Cell Rep 15:247–255. https://doi.org/10.1016/j.celrep.2016.03.025

24. Yeganeh M, Seyedjafari E, Kamrani FA, Ghaemi N (2013) RNA-binding protein Rbm47 binds to Nanog in mouse embryonic stem cells. Mol Biol Rep 40:4391–4396. https://doi.org/10.1007/s11033-013-2528-0
25. Wiederschain D The “all-in-one” system for the inducible expression of shRNA
26. Taylor SC, Nadeau K, Abbasi M, et al (2019) The Ultimate qPCR Experiment: Producing Publication Quality, Reproducible Data the First Time. Trends Biotechnol 37:761–774. https://doi.org/10.1016/J.TIBTECH.2018.12.002
27. Tomayko MM, Reynolds CP (1989) Determination of subcutaneous tumor size in athymic (nude) mice. Cancer Chemother Pharmacol 1989 243 24:148–154. https://doi.org/10.1007/BF00300234
28. Hayashi K, Lopes SMC de S, Tang F, Surani MA (2008) Dynamic Equilibrium and Heterogeneity of Mouse Pluripotent Stem Cells with Distinct Functional and Epigenetic States. Cell Stem Cell 3:391–401. https://doi.org/10.1016/J.STEM.2008.07.027/ATTACHMENT/062F78BA-63D5-4437-9C98-39F447B153FB/MMC1.PDF
29. Toyooka Y, Shimosato D, Murakami K, et al (2008) Identification and characterization of subpopulations in undifferentiated ES cell culture. Development 135:909–918. https://doi.org/10.1242/DEV.017400
30. Ying QL, Wray J, Nichols J, et al (2008) The ground state of embryonic stem cell self-renewal. Nature 453:519–523. https://doi.org/10.1038/nature06968
31. Nichols J, Silva J, Roode M, Smith A (2009) Suppression of Erk signalling promotes ground state pluripotency in the mouse embryo. Development 136:3215–3222. https://doi.org/10.1242/DEV.038893
32. Yamanaka Y, Lanner F, Rossant J (2010) FGF signal-dependent segregation of primitive endoderm and epiblast in the mouse blastocyst. Development 137:715–724. https://doi.org/10.1242/DEV.043471
33. Fossat N, Tourle K, Radziewic T, et al (2014) C to U RNA editing mediated by APOBEC 1 requires RNA -binding protein RBM 47. EMBO Rep 15:903–910. https://doi.org/10.15252/embr.201438450
34. Vanharanta S, Marney CB, Shu W, et al (2014) Loss of the multifunctional RNA-binding protein RBM47 as a source of selectable metastatic traits in breast cancer. Elife 2014:. https://doi.org/10.7554/eLife.02734.001
35. GTEx Portal. https://gtexportal.org/home/. Accessed 13 Aug 2021
36. Sampath P, Pritchard DK, Pabon L, et al (2008) A hierarchical network controls protein translation during murine embryonic stem cell self-renewal and differentiation. Cell Stem Cell 2:448–460. https://doi.org/10.1016/J.STEM.2008.03.013

Figures

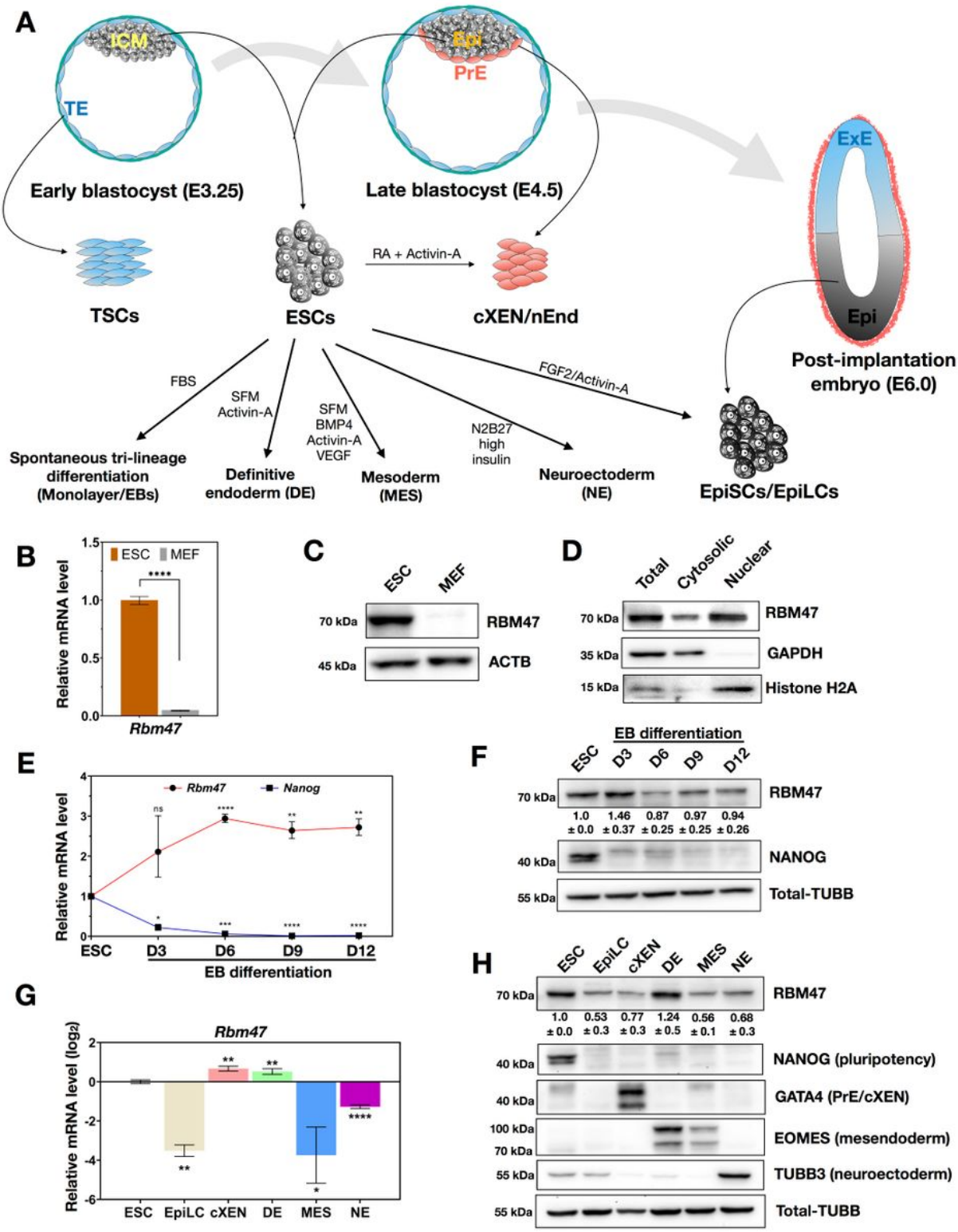

Figure 1

***Rbm47* expression is differentially regulated in mESC-based lineage specifications. A** Schematic representation of *in vitro* propagation of stem cells from TE, PrE, and ICM/Epi of a developing blastocyst and their lineage specification potential. TE- trophectoderm, ICM- inner cell mass, PrE- primitive endoderm, Epi- epiblast, TSC- Trophoblast stem cells, nEnd- naïve endoderm, cXEN- extra-embryonic endoderm, ExE- extra-embryonic ectoderm, EpiSC- epliblast stem cells. **B** RT- qPCR measurement of *Rbm47* mRNA

normalized to *Actb*, *Gapdh, and 18S rRNA* expression in indicated cell types (MEF-mouse embryonic fibroblast; ESC-AB2.2 mouse embryonic stem cells). Error bar represents the S.E.M.; N=3. **C** Western blot analysis of RBM47 in mentioned cell types. **β**-Actin (ACTB) was used as the loading control. **D** Nuclear and cytoplasmic fractionation of ESCs followed by western blotting. GAPDH was used as a cytoplasmic marker and Histone H2A was used as a nuclear marker. **E** RT-qPCR measurement of *Rbm47* mRNA during embryoid body (EB) differentiation at indicated timepoints. Values were normalized to *Actb*, *Gapdh, and 18S rRNA* expression and plotted by assaying three biological replicates (N=3). Error bars indicate S.E.M. **F** Western blot analysis of RBM47 during EB differentiation. Relative RBM47/TUBB quantification is represented as mean ± S.D from three independent blots. **G** RT-qPCR measurement of *Rbm47* mRNA in indicated lineages derived from ESCs. Values were normalized to *Actb*, *Gapdh, and 18S rRNA* expression, and $\log_2$ relative expression was plotted by assaying three biological replicates (N=3). Error bars indicate ± S.D. **H** Western blot analysis of RBM47 in indicated lineages. Lineage-specific markers were probed to confirm proper differentiation. Total **β**-Tubulin (TUBB) was used as the loading control. Relative RBM47/TUBB quantification is represented as mean ± S.D from three independent blots. Statistical test used for B, E and G- unpaired student's t-test with Welch's correction; ns- non-significant; *p<0.05; **p<0.01; ***p<0.001.

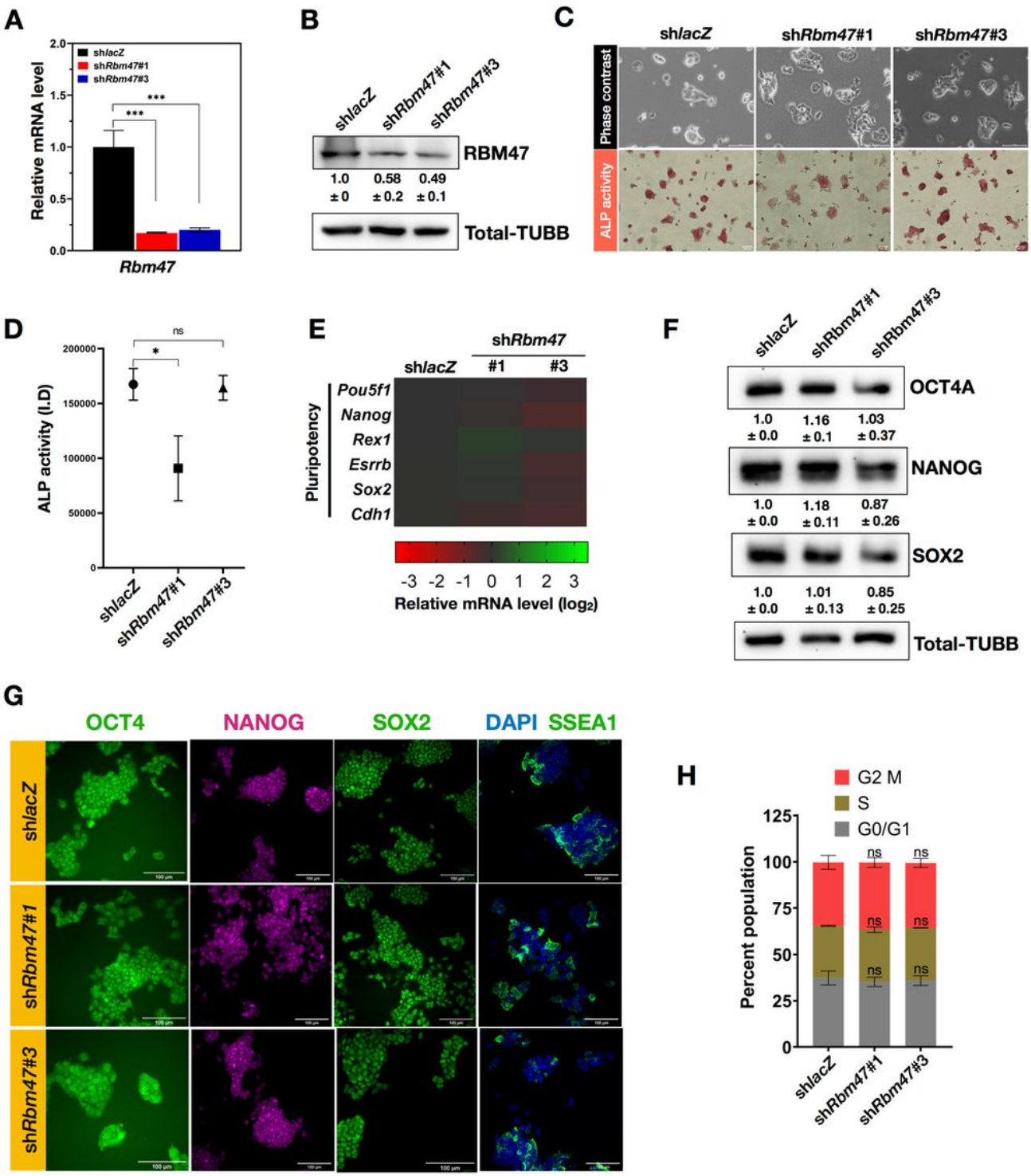

Figure 2

***Rbm47* depleted mESCs are pluripotent and can self-renew. A-B** *Rbm47*-knockdown efficiency by indicated shRNAs at RNA and protein levels. sh*lacZ* was used as a non-targeting control shRNA. **C** Phase-contrast images of sh*lacZ* ESCs and sh*Rbm47* ESCs (Top). Cells were fixed and stained for alkaline phosphatase (ALP) activity (bottom) (scale-100 μm). **D** ALP activity was quantified by calculating integrated densities (I.D) of images processed in ImageJ software. Mean integrated densities ± S.D was

plotted (N=3; >100 colonies analyzed per cell type). **E** Relative mRNA expression of indicated markers in control and sh*Rbm47* ESCs. Log_2 normalized values from three biological replicates were used for heatmap generation. **F** Western blot analysis of indicated pluripotency markers. Relative quantification is represented as mean ± S.D from three independent blots. Total-TUBB was used as the loading control. **G** Widefield fluorescence images of ESCs stained for pluripotency markers (scale-100 m). **H** Cell cycle profiling of control and sh*Rbm47* ESCs from three biological replicates. The mean percent population ± S.D was plotted. Statistical test used for A, D and H- unpaired student's t-test with Welch's correction; ns-non-significant; *p<0.05; **p<0.01; ***p<0.001.

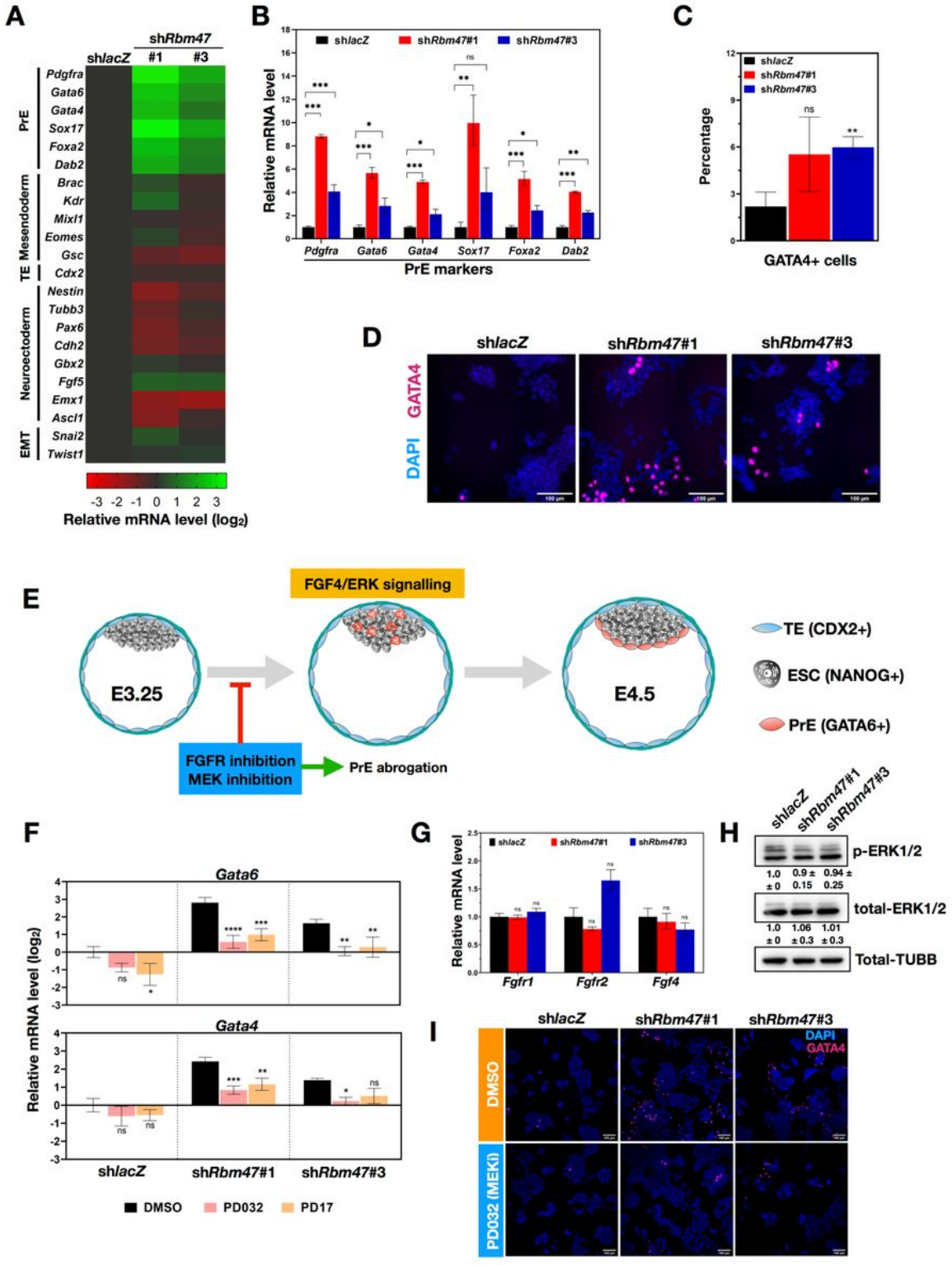

Figure 3

***Rbm47* depletion primes mESCs towards a PrE fate which is reversed by FGF-ERK pathway inhibition. A** Relative mRNA expression of indicated markers in control and sh*Rbm47* ESCs. Log_2 normalized values from three biological replicates were used for heatmap generation. **B** Relative mRNA levels of PrE markers in linear scale. **C** Quantification of GATA4+ cell population in indicated cultures using cell counter plugin of ImageJ software. Mean cell percentage ± S.D were plotted by analyzing images from three

immunostaining experiments with >1000 nuclei (DAPI) analyzed per experiment. **D** Widefield fluorescence images of ESCs immunostained for GATA4 (scale-100 μm). **E** Schematic representation of the development of early blastocyst to late blastocyst. Autocrine FGF4-ERK signaling is majorly responsible for the salt-pepper distribution of NANOG+ Epi and GATA6+ PrE specification. **F** Relative mRNA levels of *Gata6* and *Gata4* in DMSO treated, PD173074 (Pan-FGFR inhibitor) treated and PD0325901 (MEK1/2 inhibitor) treated control and *Rbm47* depleted cells (48 h treatment). Values were normalized to sh*lacZ* ESCs treated with DMSO. **G** RT-qPCR profiling of FGF receptors (*Fgfr1 and Fgfr2*) and *Fgf4* expression. **H** Immunoblotting of total ERK1/2 and p-ERK1/2 in control and *Rbm47* cell lysates. Relative quantification is represented as mean ± S.D from five blotting experiments. **I** Immunostaining of GATA4 in DMSO treated and inhibitor-treated ESCs (scale-100 m). Statistical test used for: B, C and G- unpaired student's t-test with Welch's correction; F- ordinary one-way ANOVA followed by Tuckey's test; ns- non-significant; *p<0.05; **p<0.01; ***p<0.001.

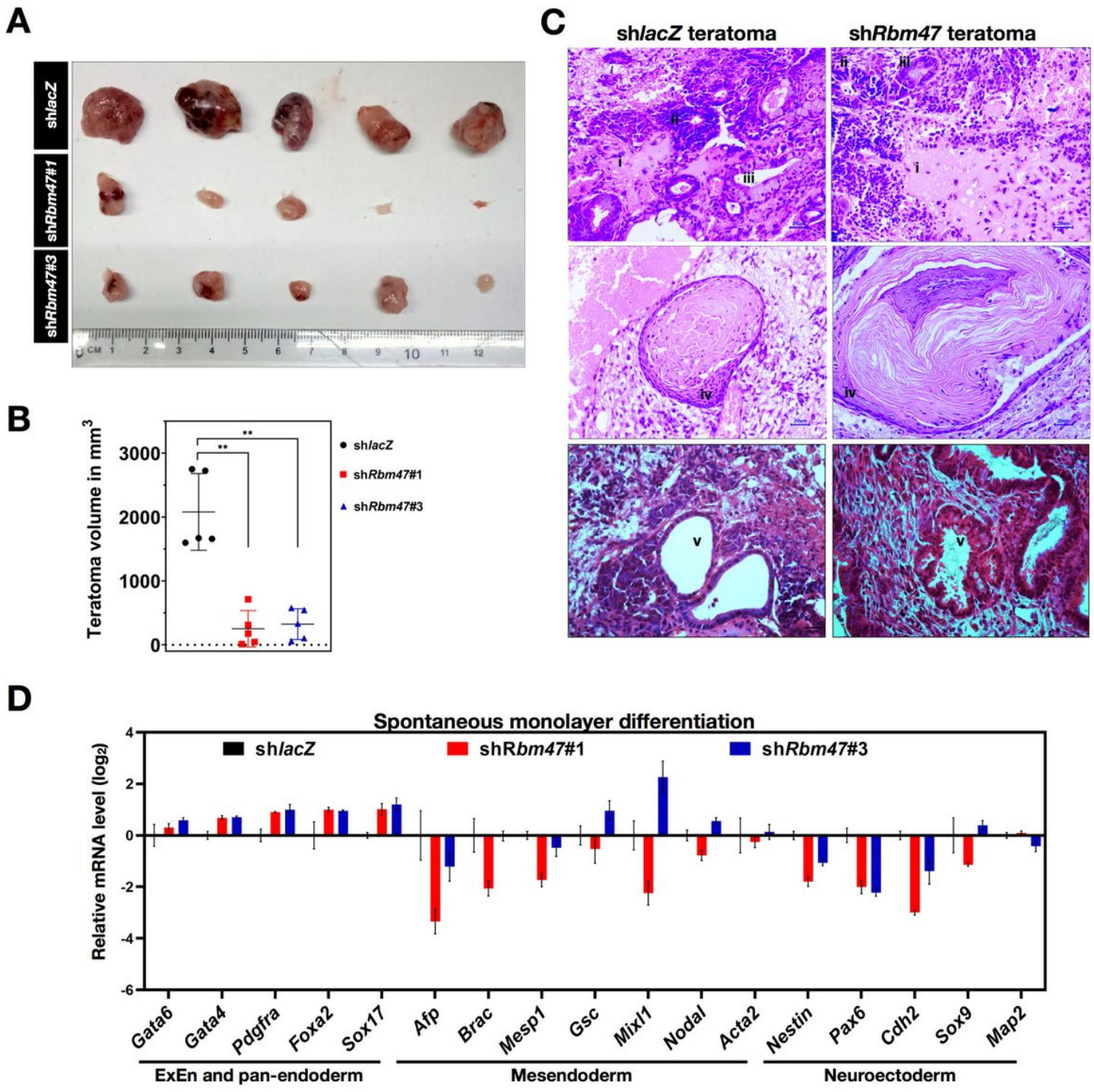

Figure 4

Depletion of *Rbm47* compromises the multi-lineage differentiation potential of mESCs. A image of the teratomas harvested from indicated NSG mice groups (N=6 for sh*lacZ*; N=7 for sh*Rbm47*#1 and #3). **B** Mean teratoma volumes were calculated to form each group. Error bars indicate S.D. **C** Representative images of HE-stained sections of teratomas from control and *Rbm47*-depleted ESCs displaying structures from three lineages: Mesoderm- osteoid/primitive bone-like (i); Ectoderm- primitive neuroepithelium (ii), a squamous epithelium with keratin pearls (iv); Endoderm- columnar epithelium/secretory glands (iii & v).

Scale bar, 20 µm. **D** RT-qPCR profiling of control and *Rbm47*-depleted ESCs differentiated for 6-days as a monolayer culture in serum-supplemented medium. Mean log2 relative mRNA expression values were plotted from two biological replicates. Statistical test used for B- unpaired student's t-test with Welch's correction; **p<0.01

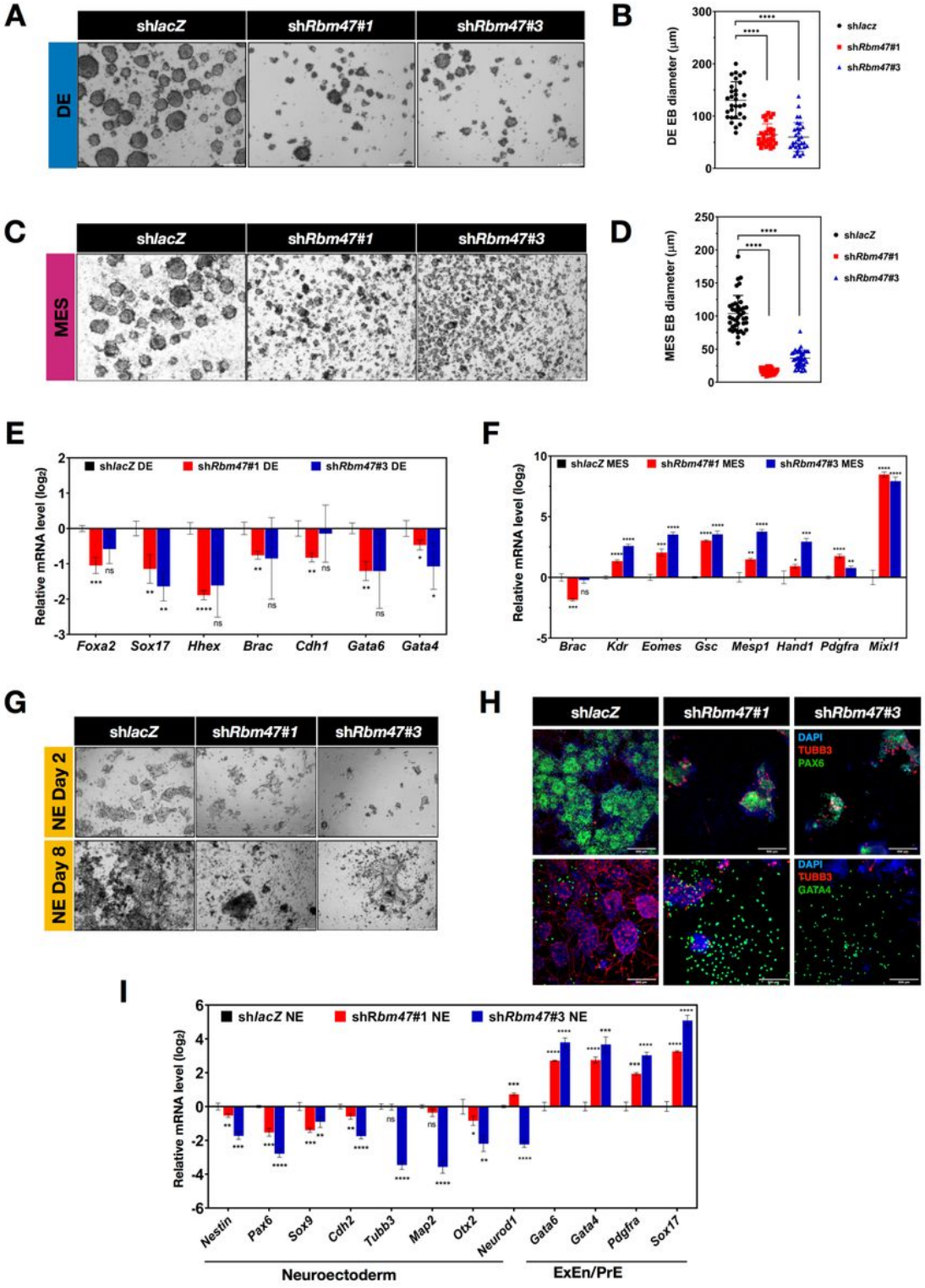

Figure 5

***Rbm47* is essential for neuroectoderm and endoderm differentiation of mESCs. A-C and G** Phase-contrast images of indicated mouse ESCs directed to DE, MES, and NE lineages. Scale bar -200 µm. **B and D** Diameter of the DE EBs (N=30) and MES EBs (N=40) were tabulated using ImageJ software and compared; mean and S.D for each cell type are represented. **E, F, and I** RT-qPCR profiling of control and sh*Rbm47* ESCs differentiated into a specific lineage. Mean log2 relative expression values were plotted from three biological replicates (N=3). **H** Immunostaining of control NE and sh*Rbm47* NE with PAX6, TUBB3, and GATA4 antibodies. Widefield fluorescent images were acquired in the ThermoFisher CellInsight-high content screening platform. Scale bar, 500 µm. Statistical test used for: B and D- unpaired student's t-test with Welch's correction; E, F and I- multiple t-tests using Holm-Sidak method; ns- non-significant; *p<0.05; **p<0.01; ***p<0.001.

Supplementary Files

This is a list of supplementary files associated with this preprint. Click to download.

- Supplementaryinformation.pdf